Applied Catalysis A, General 570 (2019) 283–291

Contents lists available at ScienceDirect

Applied Catalysis A, General

journal homepage: www.elsevier.com/locate/apcata

Operando HERFD-XANES/XES studies reveal differences in the activity of Fe-species in MFI and CHA structures for the standard selective catalytic reduction of NO with NH_3

Miren Agote-Arán[a,b,c], Inés Lezcano-González[a,b], Alex G. Greenaway[a,b], Shusaku Hayama[c], Sofía Díaz-Moreno[c], Anna B. Kroner[c], Andrew M. Beale[a,b,*]

[a] Chemistry Department, University College of London, Gordon Street, London, WC1H 0AJ, UK
[b] Research Complex at Harwell, Rutherford Appleton Laboratory, Didcot, OX110FA, UK
[c] Diamond Light Source Ltd, Harwell Science and Innovation Campus, Didcot, OX11 0DE, UK

ARTICLE INFO

Keywords:
NH_3-SCR
NO
Fe-containing zeolites
HERFD-XANES
XES

ABSTRACT

Fe-containing zeolites were studied as catalysts for the standard NH_3-SCR reaction with the primary aim of gaining insight into the structure-function relationship of these materials. Catalysts with different Fe nuclearity (i.e. isolated species, clusters, large particles) were synthesised by incipient wetness impregnation, using H-ZSM-5, H-SSZ-13 and Silicalite-1 as supports, and characterised by in situ and operando X-ray emission spectroscopy (XES) and high energy resolution fluorescence detected X-ray absorption near-edge spectroscopy (HERFD-XANES) under NH_3-SCR conditions. The combination of these techniques allowed us to obtain a detailed understanding of the changes in Fe coordination, oxidation state and geometry occurring during reaction. The results obtained suggested that isolated octahedral Fe^{3+} species on H-ZSM-5 are highly active under the conditions studied, undergoing reduction when exposed to NH_3 or under SCR conditions. In contrast, isolated tetrahedral Fe^{3+} sites present in Silicalite-1 exhibited lower redox properties, leading to a reduced NO conversion. Clusters and Fe_xO_y particles on H-SSZ-13 exhibited low SCR activity.

1. Introduction

Nitrogen oxides (NO_x) are one of the major sources of air pollution produced from engines during fuel combustion processes. Today selective catalytic reduction of NO with ammonia (NH_3-SCR) is a widely applied technology for converting the NO_x emissions from diesel engines into harmless N_2 and H_2O.

Fe-containing zeolites are among the most active catalysts for NH_3-SCR [1,2]. Much research has been devoted to study catalyst preparation methods towards optimum activity [3–10] as well as to investigate the relationship between structure and activity of the different Fe species [12–18]. These studies are however challenging, mostly due to the presence of many Fe species (i.e. isolated species, oligomers or large particles) on the catalysts and the difficulties to unequivocally characterise them. Thus, isolated Fe cations, binuclear species or Fe clusters have been proposed as the most active centres by different groups. Among the isolated Fe centres, tetrahedral (Td) Fe^{3+} species were initially reported to be the most active sites [8], while more recent studies suggest that isolated octahedral (Oh) and distorted Td Fe^{3+} are more active than Td Fe^{3+} centres [11]. Furthermore, it has been proposed that all Fe species show some NH_3-SCR activity and that NO conversion rates depend on the reaction temperature; monomeric species are responsible for SCR $< 300\,^{\circ}C$, with increasing contributions of dimeric and oligomeric species at higher temperatures and even of Fe_2O_3 particles $> 500\,^{\circ}C$ [13].

Debate is also ongoing regarding the reaction mechanism on Fe/zeolites. Many research groups support oxidative NO activation by Fe^{3+} resulting in an adsorbed NO_x intermediate; NO_x then reacts with NH_4^+ - adsorbed either over Fe^{3+} or the zeolite Brønsted acid sites (BAS) [18–20], forming NH_4NO_2 which decomposes to N_2 and H_2O. An alternative mechanism proposes that NH_3 is first adsorbed on Fe^{3+} giving an Fe^{2+}-NH_2 intermediate. Fe^{2+}-NH_2 then reacts with NO in the gas phase yielding N_2 and H_2O, and leaving a reduced Fe^{2+} centre [21]. Initially, oxidation of NO to NO_2 was proposed as the rate-determining step in the standard SCR mechanism [1,22–25]; however, recent studies have shown a lack of correlation between the rates of NO_2 formation and standard SCR [26]. In their in situ XANES studies, Høj et al. [17] observed a higher reduction degree of Fe with increasing NO

* Corresponding author at: Chemistry Department, University College of London, Gordon Street, London, WC1H 0AJ, UK.
E-mail address: andrew.beale@ucl.ac.uk (A.M. Beale).

https://doi.org/10.1016/j.apcata.2018.11.026
Received 18 September 2018; Received in revised form 9 November 2018; Accepted 26 November 2018
Available online 27 November 2018

conversion, leading to the proposal that the rate limiting step must be associated to the reoxidation of Fe^{2+} to Fe^{3+}.

The role of BAS on Fe/zeolites has also been largely discussed. On the basis of reports showing an increased SCR activity with increasing BAS density [7,24,27], it has been proposed that NH_4^+ ions formed on the BAS act as ammonia reservoir in the vicinity of the active Fe centres [28]; alternatively, BAS could also have a role in catalysing the decomposition of NH_4NO_2 [29]. Contrary to these hypotheses recent studies suggest that acidity is not a decisive factor for good NH_3-SCR activity [27]; in line, temperature programmed desorption and infrared spectroscopy studies point that BAS are not required for activation of adsorbed NH_3 [30]. The higher activity in acidic zeolites is thus attributed to their role on Fe dispersion into highly active isolated species.

Catalyst improvement for the control of NO_x emissions requires a better understanding of the effect of Fe speciation on the catalytic activity, as well as further insight into the NH_3-SCR reaction mechanism. To this end, a set of Fe/zeolites (~ 0.5 wt. %) were prepared using different Fe precursors (i.e. Fe nitrate or Fe citrate) and zeolite supports. The supports studied were H-ZSM-5 (MFI structure, Si/Al = 15), H-SSZ-13 (CHA structure, Si/Al = 15) and Silicalite-1 (MFI structure, Si/Al = ∞). The Silicalite-1 here used was post-treated after synthesis to generate a large population of silanol groups forming nests; these framework defects are generated by the extraction of framework Si^{4+} and constitute vacant framework sites, known to serve as grafting sites for Fe^{3+} and allowing a good dispersion [31]. The preparation methods used led to catalysts with different Fe species distribution and varying population of acid sites (i.e. with and without BAS). The catalytic activity of these materials was compared while the structure of Fe centres was studied by high energy resolution fluorescence detected X-ray absorption near-edge (HERFD-XANES) and X-ray emission spectroscopy (XES).

Analysis of the Fe K-edge X-ray absorption spectra is an attractive way to gain information on the structure of Fe species. In particular, both position and intensity of the pre-edge peak (arising from 1 s→3d electronic transition) are sensitive to the oxidation state and coordination geometry of Fe species [32–34]. Collecting XANES in HERFD mode results in increased spectral resolution allowing for a detailed pre-edge analysis for qualitative and quantitative Fe speciation studies [18,35,36]. The narrow fluorescence energy bandwidth selected by the high-resolution spectrometer can overcome the core-hole lifetime broadening [37]; this suppresses unwanted background level [37] giving sharper spectral features and a greater separation of the pre-edge structure from the main edge as compared to conventional absorption spectroscopy. The non-resonant XES studies in this work were centred in the analysis of the Kβ mainlines (3p → 1 s electronic transition), sensitive to the Fe valence spin and oxidation state, as well as the ionicity of metal-ligand bonds [38].

Furthermore, the spectra collection was carried out in situ and under operando conditions by exposing the catalysts to NO, NH_3 and standard NH_3-SCR conditions (with O_2, NH_3 and NO as the reactants), this allowed to follow changes in Fe sites under different gas environments. The results enable to further evaluate the relevance of different Fe speciation and the Brønsted acidity in Fe/zeolite catalysts for the standard NH_3-SCR reaction.

2. Materials and methods

2.1. Catalyst preparation

ZSM-5 zeolite with MFI structure (Si/Al = 15) was purchased from Zeolyst (CBV3024E) in its ammonium form. The proton form of the material was obtained by calcination in static air at 550 °C for 6 h, the heating rate used was 2 °C/min. Silicalite-1, was prepared by hydrothermal synthesis as described by Lobo et al. [39] and calcined at 550 °C for template removal. Silicalite-1 was treated with ethylenediamine following the procedure reported by Wang et al. [40] in order to generate silanol nests in the structure by the extraction of framework Si^{4+}. The resulting Silicalite-1 is named as S1-T. H-SSZ-13 with CHA structure (Si/Al = 15) was prepared by hydrothermal method in fluoride media following previously reported methods [41–43]. The sample was calcined in air with the following temperature program: 1 °C min^{-1} to 120 °C, held for 2.5 h; 2.2 °C min^{-1} to 350 °C, and 3 h at this temperature; and finally 0.8 °C min^{-1} to 580 °C, and held for 3 h.

Fe-containing zeolites with metal loadings of ~ 0.5 wt. % were prepared by incipient wetness impregnation using either ferric nitrate ($Fe(NO_3)_3.9H_2O$, Sigma Aldrich, 99.95%) or ammonium iron citrate ($C_6H_8O_7{\cdot}xFe_3^+{\cdot}yNH_3$, Sigma Aldrich, 16.5–18.5% Fe) as precursors. After impregnation the samples were dried overnight at 60 °C and calcined at 500 or 800 °C for 3 h (the heating rate was 5 °C/min). A Fe/Silicalite-1 was prepared using ferric nitrate and calcined in air at 500 °C, this sample is denoted as Fe/S1-T-nitr. A second Fe/Silicalite-1 was synthesised using ferric citrate with calcination at 800 °C (coded as Fe/S1-T-citr). Medium pore Fe/H-ZSM-5 and small pore Fe/H-SSZ-13 were also prepared following this latter procedure.

2.2. Catalyst characterisation

Powder X-ray diffraction (XRD) patterns were recorded using a Rigaku SmartLab X-Ray Diffractometer fitted with a hemispherical analyser. The measurements were performed using Cu Kα radiation source (λ = 1.5406 Å) with a voltage of 40 kV, and a current of 30 mA. The patterns obtained were compared to crystallographic data in the reference library (ICSD database).

Fourier-transform infrared spectroscopy (FTIR) spectra were recorded in a Nicolet iS10 spectrometer. Samples were pressed into self-supporting wafers with a density of c.a. 10 mg/cm^2. The wafers were dried prior the measurements by heating them up to 285 °C for 3 h under 70 ml/min He flow. After dehydration, the sample was cooled down to 150 °C under dry He for the spectra collection.

Temperature programmed desorption of ammonia (NH_3-TPD) was performed in an AutoChem II 2920 micromeritics instrument equipped with a moisture trap and a thermo-conductivity detector. Samples were first preactivated by flowing pure N_2 and heating up to 550 °C for 30 min (5 °C/min). The reactor was then cooled down to 100 °C for ammonia absorption which was run by flowing 1% NH_3/N_2 until saturation (~ 1 h). Next, pure N_2 was flowed for 2 h to remove any excess of NH_3 on the sample. Finally, NH_3 desorption was carried out by increasing temperature up to 1100 °C with a heating rate of 10 °C/min. All the signals were normalised to the sample mass.

UV-Vis diffuse reflectance measurements were carried out ex situ in an UV-2600 Shimadzu spectrometer, using a light spot of 2 mm. The reflectance data was acquired from 200 to 800 nm which was transformed into absorbance versus wavelength by applying the Kubelka-Munk equation. $BaSO_4$ was used as white standard to remove background.

Chemical analysis was carried out using inductively coupled plasma optical emission spectroscopy (ICP-OES) in a Perkin Elmer Optical Emission Spectrometer Optima 3300 RL.

2.3. Catalytic tests

Catalyst testing was carried out by introducing 0.20 g of sieved catalyst (150–425 μm sieved fraction) into a tubular quartz reactor (ID 0.7 cm), the catalyst bed was fixed in the isothermal zone of the oven by quartz wool. The sample was first activated by heating at 500 °C for 1 h under 20% O_2/He flow; the heating rate used was 5 °C/min. The sample was then cooled down to 300 °C under pure He. Once at 300 °C, NH_3-SCR reaction was performed for 1 h by flowing 200 mL/min (GHSV = 35,000 h^{-1}) of 5000 ppm NO, 5000 ppm NH_3 and 5% O_2 in He. Pfeiffer Vacuum OmniStar, GSD 301 quadrupole mass spectrometer

was used for the online gas analysis.

2.4. In situ and operando HERFD-XANES and XES

HERFD-XANES/XES measurements were carried out at Diamond Light Source (Harwell Campus, UK) at the scanning branch of I20 beamline [44,45]. The beamline is equipped with an Si (111) Scanning Four Bounce monochromator [46] for selecting the incident X-rays energy. The X-ray emission spectrometer based on a 1 m diameter Rowland circle operating in the Johann configuration in the vertical plane [47] was used for the experiment. The spectrometer was equipped with three 100 mm Si (531) spherical analyser crystals for the analysis of the fluorescence signal.

The beam size at the sample was ~ 400 x 400 µm (HxV) FWHM. The X-ray absorption spectra in terms of HERFD-XANES were measured by scanning the incident energy (7062–7400 eV) and detecting the fluorescence at the maximum of the Fe $K\beta_{1,3}$ emission line (7059.25 eV) with the energy resolution better than the core-hole life-time of Fe K-edge. The X-ray emission spectra around Kβ′ and $K\beta_{1,3}$ emission lines were recorded between 7020 and 7130 eV while applying an excitation energy of 7212 eV, far above the K-edge energy of Fe (7112 eV). The emission lines were normalised to the $K\beta_{1,3}$ spectral intensity.

The Fe/zeolite samples were measured under flowing gas using a heated borosilicate capillary as the microreactor (diameter 1.5 mm, wall thickness ~ 10 µm). Around 15 mg of sample were fixed in the capillary using quartz wool, the capillary was mounted over a hot air blower and gas mixtures were dosed with mass flow controllers to obtain the desired volume concentrations. First the catalyst was activated by heating at 500 °C for 1 h under 20% O_2/He flow, then the sample was cooled down to 200 °C in He. Once the temperature of 200 °C was achieved, 40 mL/min (GHSV = 120,000 h^{-1}) of 0.1% NO/He or 1% NH_3/He were flown through the reactor. Finally, operando NH_3-SCR measurements were performed at 300 °C by flowing 100 mL/min (GHSV = 300,000 h^{-1}) of 0.5% NO, 0.5% NH_3 and 5% O_2 in He. For Fe/H-SSZ-13, only the activation and NH_3-SCR steps were performed; with this catalyst a larger amount of sample (~ 25 mg) was used which resulted in lower GHSV of around 180,000 h^{-1} for the operando NH_3-SCR experiments. Between each adsorption or SCR experiments the sample was reactivated by heating at 400–500 °C in air for 1 h. All heating rates employed were 5 °C/min. A Pfeiffer Vacuum OmniStar, GSD 301 quadrupole mass spectrometer was used for the online gas analysis.

The following references were measured ex situ: Fe_2O_3 (Sigma Aldrich, 99.995%), $FeSO_4.7H_2O$ (Sigma Aldrich, 99.990%), $FePO_4.2H_2O$ (Sigma Aldrich, 29% Fe) and $FePO_4$ (obtained by calcination of $FePO_4.2H_2O$ at 400 °C for 6 h). The references where diluted in cellulose to minimise self-absorption aiming for ~ 0.5 wt. % loading of Fe and then pressed into pellet form for the spectra collection.

Normalisation and HERFD-XANES data processing were carried out using the Athena software [48]. For a detailed analysis of the pre-edge peak features the contribution of the main Fe K-edge in the pre-edge region was determined using Origin 9.1 software and using a cubic spline function obtained by interpolating the data several eV before and after the pre-edge. The subtraction of the modelled main edge contribution from the XANES spectra over the full energy ranges yields the isolated pre-edge feature. The pre-edge spectral shape was deconvoluted with $R^2 > 0.997$ using gaussian components. Contributions > 7115 eV were excluded for the total area and centroid position calculations as the intensity in this region correspond to Fe-Fe scattering contributions and bring no relevant information regarding oxidation state or coordination symmetry. The spectra collection time was 12 min for HERFD-XANES and 20 min for XES. The possibility of beam-induced damage was ruled out by ensuring no spectral changes occurred in consecutive scans under the same sample environment.

Table 1
Chemical analysis results for Fe/zeolites synthesised using different zeolite topologies and Fe precursors.

Sample	Fe (wt. %)	Al (wt. %)	Si (wt. %)	Si/Al	Fe/Al
Fe/H-ZSM-5	0.74	2.45	40.70	15.9	0.14
Fe/S1-T-citr	0.48	/	/	/	/
Fe/S1-T-nitr	0.51	/	/	/	/
Fe/H-SSZ-13	0.53	2.27	35.00	14.8	0.11

3. Results and discussion

3.1. Fe/zeolites characterisation

The elemental analysis carried out for all Fe/zeolites studied is shown in Table 1. Fe content of the samples is between 0.48 to 0.74 wt. %. Al content is comparable for H-ZSM-5 and H-SSZ-13 zeolites with Si/Al ratio of 16 and 15 respectively.

UV-Vis spectroscopy was used to investigate the nature of Fe^{3+} species by observation of the $Fe^{3+} \longleftarrow O^{2-}$ ligand to metal charge-transfer bands (Fig. 1). Absorption between 215 and 300 nm has previously been attributed to the presence of isolated Fe^{3+} species; bands between 215 to 240 nm are typically associated with Fe^{3+} in tetrahedral coordination while bands between 250 to 300 nm are ascribed to Fe^{3+} in octahedral coordination [49]. Absorption between 300 and 400 nm arise from Fe_xO_y clusters in an octahedral environment while absorption > 450 nm corresponds to large Fe_2O_3 particles outside the zeolite pores [49].

As designed by the use of different Fe precursors and zeolite supports, UV–vis spectra revealed that the syntheses resulted in catalysts with different Fe speciation. For Fe/H-ZSM-5 (with BAS associated to framework Al) and Fe/S1-T-citr (with no BAS), most of the absorption occurs below 300 nm which can be attributed to isolated Fe species. Unlike for Fe/S1-T-citr, two distinct bands can be observed on Fe/H-ZSM-5 with maxima at 220 and 272 nm, suggesting presence of both tetrahedrally and octahedrally coordinated Fe^{3+} on the acidic zeolite [49]. The good Fe dispersion obtained using ammonium Fe citrate precursor can be attributed to the chelating effect of the bulky citrate ligand which keeps Fe centres separated resulting in isolated Fe^{3+} upon calcination of the ligand.

Compared to Fe/S1-T-citr, the catalyst prepared with nitrate precursor (Fe/S1-T-nitr) presents a weaker absorption below 300 nm and increased absorption intensity at 345 and 493 nm, suggesting a lower Fe dispersion and the formation of Fe_xO_y clusters and large Fe_2O_3

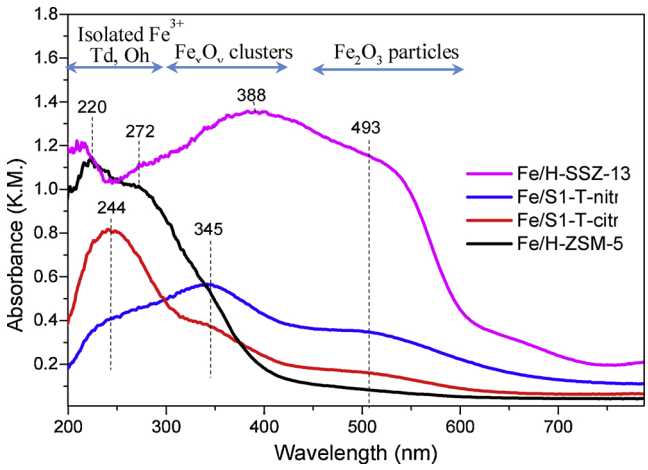

Fig. 1. UV–vis absorption spectra of Fe/zeolites (0.5 wt. %) synthesised using different zeolite topologies and Fe precursors.

particles. As expected, Fe/H-SSZ-13, a small-pore zeolite material, exhibits intense bands between 400 and 650 nm pointing out to the presence of large Fe_2O_3 particles. Nonetheless, absorption < 250 nm suggests some Fe to be present as isolated species, probably in tetrahedral symmetry. The formation of clustered and Fe_2O_3 particles when using H-SSZ-13 as support might be due to the smaller pore size of this material (3.8 Å) as compared to the size of the Fe-citrate precursor (~ 5.5 x 6.7 Å) [50]; i.e. the precursor is too bulky to enter and disperse into the pores during the impregnation process, leading to the formation of Fe oxide particles on the external zeolite surface.

Also, for verifying that aimed zeolite framework structures and acidic properties were obtained, the synthesised zeolites where characterised by powder X-ray diffraction (XRD), Fourier-transformed infrared spectroscopy (FTIR) and ammonia temperature programmed desorption (NH_3-TPD). The characterisation results can be found in Fig. S1 in the electronic supporting information (ESI).

3.2. In situ and operando HERFD-XANES/XES

3.2.1. HERFD-XANES and XES analysis of Fe references and the activated Fe/zeolite samples

In order to gain further insight into the oxidation state and geometry of the Fe species present on the as-prepared catalysts, Fe K-edge HERFD-XANES measurements were performed at room temperature after in situ activation at 500 °C (20% O_2/He). The integrated intensity and energy position of the pre-edge peak are correlated using a scatter plot. The points corresponding to the pre-edge spectra of model reference compounds (i.e. with known oxidation states and coordination geometries) have unique coordinates in such a plot. These coordinates can be used for qualitative and quantitative analysis of Fe species in unknown compounds such as Fe/zeolites [32,34].

Normalised HERFD-XANES spectra are shown in Fig. 2a together with the spectra of different Fe references; detailed features of the pre-edge region are shown in Fig. 2b. For better visualisation of Fe structural properties, the pre-edge peak intensity vs. centroid position scatter plot resulting from the pre-edge peak isolation and analysis is shown in Fig. 3. The isolated deconvolution plots can be found in Figs. S2 and S3 in the ESI while the resulting component, centroid and integrated intensity values are shown in Table S1.

If we first compare the HERFD-XANES features of reference compounds, simple visualisation of the spectra in Fig. 2 shows that Fe_2O_3 exhibits increased spectral intensity between the pre-edge peak and the absorption edge (i.e. from 7115 to 7120 eV, labelled as Fe-Fe in Fig. 2b). The Fe_2O_3 structure comprises interconnected FeO_6 octahedral units, and this contribution is attributed not to electronic transitions but to a neighbouring Fe-Fe scattering effect [32]. Consequently, a lower intensity is observed in this region for $FePO_4$, $FePO_4.2H_2O$ and $FeSO_4.7H_2O$ references, which consist of FeO_x units isolated by phosphate or sulphate groups.

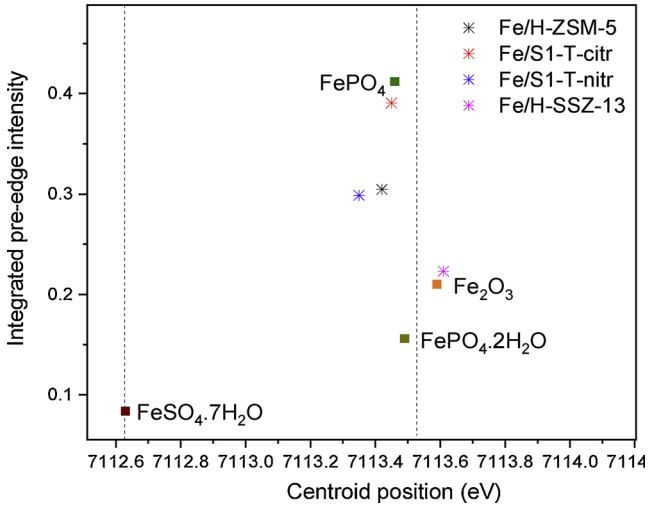

Fig. 3. Pre-edge integrated area vs area-based average centroid for Fe in selected reference compounds and Fe/zeolite samples. Dotted vertical lines around 7112.6 and 7113.5 eV indicate the average energy position of the centroid for Fe^{2+} and Fe^{3+} compounds respectively.

The integrated pre-edge peak intensity and shape is indicative of metal coordination symmetry; it is known to increase for non-centrosymmetric species (i.e. tetrahedral) due to the higher degree of 3d–4p hybridisation in such geometries [18]. Accordingly, as seen in Figs. 2 and 3, $FePO_4$ comprising isolated Td Fe^{3+} units, exhibits a sharp and strong pre-edge peak with integrated area of 0.42 (see Table S1 for the values of integrated areas). $FePO_4.2H_2O$ and Fe_2O_3 exhibit a two-component pre-edge peak (with maxima around 7113.0 and 7114.5 eV) characteristic of Oh Fe^{3+} compounds [34]. As expected for geometries with inversion symmetry, these references present a weaker integrated intensity. Note, the slight pre-edge intensity increase from $FePO_4.2H_2O$ to Fe_2O_3 with integrated areas of 0.16 and 0.21 respectively (Table S1); this is attributed to the highly distorted Oh structure of Fe^{3+} in Fe_2O_3 (with three short and three long Fe-O bonds) [51] which deviates significantly from being centrosymmetric.

$FeSO_4.7H_2O$ with Oh Fe^{2+} also exhibits a two-component weak pre-edge peak; nonetheless the maxima of these are shifted to lower energies (to 7111.3 and 7113.3 eV) as a result of the lower Fe oxidation state. Thus, while all ferric references exhibit the pre-edge peak centroid around 7113.5 eV the centroid for the ferrous reference appears at 7112.6 eV. Note here that the integrated pre-edge area for $FeSO_4.7H_2O$ (0.083) is lower than for the ferric compounds studied. As the Fe_2O_3/$FeSO_4.7H_2O$ area ratio obtained (c.a. 2.5) is comparable to previous reports [32,52], the decreased intensity in the ferrous reference can be

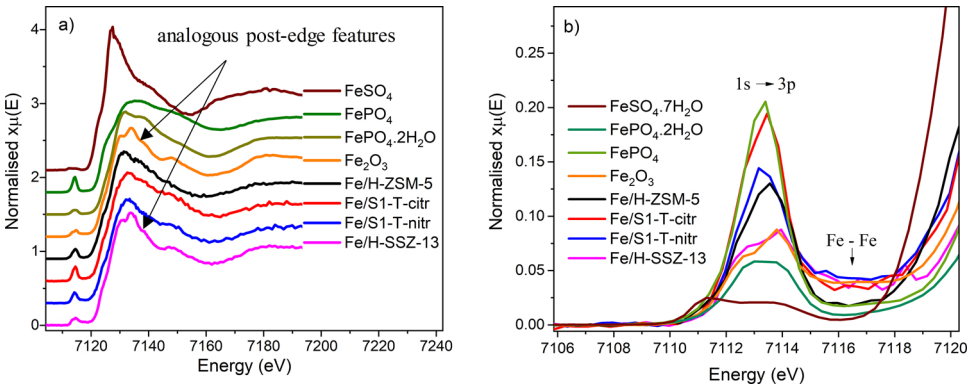

Fig. 2. Fe K-edge HERFD-XANES spectra of Fe references and Fe/zeolites (at RT after calcination in flowing air at 500 °C): a) Full XANES region and b) the pre-edge region.

explained by the lower probability of 1s→3d transition for reduced Fe^{2+} due to its more populated 3d orbital. Low degree of distortion in its octahedral FeO_6 units in this reference probably also contributes to the weak peak intensity [53].

Considering the spectral features of the reference compounds discussed above, structural information on Fe species in the catalysts can be extracted by comparative analysis of HERFD-XANES. Thus, data in Fig. 2a show a featureless post-edge for Fe/H-ZSM-5, Fe/S1-T-citr and Fe/S1-T-nitr suggesting that Fe species exhibit low long-range order (i.e. isolated species or small clusters). Fe/H-SSZ-13 however, exhibits a lower pre-edge peak intensity and pronounced post-edge features resembling those of Fe_2O_3. This is consistent with the UV–vis data showing the presence of large Fe_2O_3 particles on the zeolite outer surface. Conversely, Fe/H-ZSM-5 shows a larger number of isolated Fe species, as seen by the lower intensity between the pre-edge and the rising absorption edge (see Fe-Fe contribution in Fig. 2b). The higher intensity in this region for Fe/S1-T-citr, Fe/S1-T-nitr and Fe/H-SSZ-13 implies the presence of Fe_xO_y clusters or particles resulting in Fe-Fe contribution to the spectra.

From the study of the pre-edge peaks centroid position in Fig. 3, all Fe/zeolites display the centroid around 7113.5 eV, close to the values reported for ferric references, evidencing predominance of Fe^{3+} species. If we analyse the pre-edge integrated area, Fe/H-ZSM-5 (0.30) sits between $FePO_4$ (0.42) and Fe_2O_3 (0.21) references. This intermediate pre-edge intensity has been ascribed to 5-fold Fe species by some groups [35]. In our studies however, this intensity can be better attributed to the presence of a mixture of isolated Td and Oh like Fe^{3+} species, as indicated by the UV–vis spectra discussed in Fig. 1.

Taking into account previous studies on Fe/H-ZSM-5 by Lobree et al., it can be argued that with the low Fe/Al ratios used here, isolated Fe^{3+} species exchange Brønsted acidic protons on a one-to-one basis [54]. It has been reported that isolated Fe species can be located in different MFI framework sites (i.e. α, β or γ sites) [54]. Many monomeric Fe sites have been proposed by theoretical modelling studies and the final Fe coordination and geometry varied according to specific framework location or zeolite Al distribution [55,56]. In the present study, we cannot readily provide any further information on the structure/location of the extra-framework isolated Fe species.

The intense pre-edge on Fe/S1-T-citr (integrated area 0.39) suggests that tetrahedral Fe^{3+} species are predominant. This can be explained by the high density of silanol groups forming nests (i.e. framework vacancies) in S1-T zeolite - as verified by FTIR shown in Fig. S1 in the ESI, leading to the incorporation of Fe^{3+} in framework positions adopting Td geometry. In addition, the absorption between the pre-edge and the rising absorption edge (Fig. 2b) indicates an Fe-Fe contribution that can be attributed to the presence of minor Fe_xO_y clusters and Fe_2O_3 particles as observed by UV–vis.

Fe/S1-T-nitr shows a pre-edge peak intensity between those of the Oh and Td references as well as the presence of an Fe-Fe contribution between the pre-edge and the rising absorption edge. This is again in agreement with the UV–vis results which suggests the presence of isolated Fe^{3+} species that would possess Td symmetry (consistent with the highly defective S1-T), as well as the presence of both small clusters and Fe_2O_3 particles. Finally, Fe/H-SSZ-13 exhibits pre-edge peak features and an intensity analogous to the Fe_2O_3 reference, indicating clear predominance of large Fe oxide particles, likely located on the zeolite outer surface [33].

The intensity of the pre-edge is known to be inversely correlated with the extent of centrosymmetry of the crystallographic site of Fe [32]. Thus, assuming a linear relationship between pre-edge intensity and the number of Td Fe^{3+} centres, a rough quantification of the species present can be performed to estimate the fraction of Td species in the sample (see Equation S1 in ESI for further details on the quantification). The results, presented in Table 2, indicate that approximately 45%, 86%. 42% and 9% of Td Fe^{3+} species are present in Fe/H-ZSM-5, Fe/S1-T-citr, Fe/S1-T-nitr and Fe/H-SSZ-13 respectively. This estimation is in good agreement with quantification carried out by linear combination analysis (LCA) of the pre-edge spectra fitting with $FePO_4$ and Fe_2O_3 as the references for Td and Oh Fe^{3+} species. These results are also shown in Table 2 while fitted spectra are included in Fig. S4 of the ESI. From the LCA there is a 44% contribution of Td Fe^{3+} in Fe/H-ZSM-5, 88% in Fe/S1-T-citr and 48% in Fe/S1-T-citr. Fitting of Fe/H-SSZ-13 gives 100% contribution of Oh Fe^{3+} with negligible Td Fe^{3+}.

Table 2
Quantification of Oh and Td Fe^{3+} centres in Fe/zeolites (spectra at room temperature after calcination under 20% O in He at 500 °C) by pre-edge integrated intensity values as well as by linear combination of the pre-edge region (-15 to -5 eV from the main adsorption edge) using $FePO_4$ and FeO_3 spectra as the Fe^{3+} Td and Fe^{3+} Oh references.

Sample	Pre-edge intensity Weight fraction Fe^{3+} Td	LCA Weight fraction Fe^{3+} Td	LCA Weight fraction Fe^{3+} Oh	LCA R (%)
Fe/H-ZSM-5	0.45	0.44	0.56	2.7
Fe/S1-T-citr	0.86	0.88	0.12	2.8
Fe/S1-T-nitr	0.42	0.48	0.52	2.2
Fe/H-SSZ-13	0.09	0.00	1.00	2.1
Fe/H-ZSM-5[a]	0.55	0.48	0.52[a]	2.6

[a] Analysis of Fe/H-ZSM-5 using $FePO_4.2H_2O$ as the Fe^{3+} Oh reference.

According to UV–vis results discussed in Fig. 1, Fe/H-ZSM-5 appears to be composed mainly by isolated Fe species; hence, the analysis of this sample is performed by using $FePO_4.2H_2O$ (which comprises isolated FeO_6 units) as Oh Fe^{3+} reference. The results, included in Table 2, show that the choice of the reference introduces variation of up to 10% in the quantification of Fe species. Also, it needs to be taken into account that in the quantification of Fe^{3+} species in Oh and Td coordination we cannot completely rule out minor effects due to the presence of water traces; this would result in a certain increase in the amount of Oh sites, especially in the case of isolated metal sites.

In addition to the HERFD-XANES data discussed above, the Kβ XES spectra were also acquired. Fig. 4 shows the Kβ' and $K\beta_{1,3}$ mainlines (3p→1s transitions of the absorbing atom) for references and Fe/zeolites (room temperature after calcination). All the spectra present a well-defined Kβ' feature indicating they constitute high-spin complexes [57].

Recent publications report that Kβ' and $K\beta_{1,3}$ spectra can reveal more than the spin-state of a material. For metal complexes with the same spin-state, the centroid of the $K\beta_{1,3}$ feature can be correlated with the covalent (vs. ionic) character of the metal-ligand bond; it has been reported that $K\beta_{1,3}$ emission shifts to higher energies with increasing ionic character [38]. This is seen in the high-spin references shown in Fig. 4a (see inset for better visualisation of the position of the $K\beta_{1,3}$ line). The ionic character of a given metal-ligand bond in transition metal complexes can be inferred from the bond distance (i.e. increasing ionic character for increasing bond distance). $FeSO_4.7H_2O$ is an ionic compound [58], and although in a lower oxidation state, the longer average Fe-O distances (2.12 Å) [59] ensure a lower covalent character. Consistently, the maxima of the $K\beta_{1,3}$ peak for this reference is positioned at the highest energy (7059.44 eV). $FePO_4$ with a shorter average Fe-O bond distance (1.85 Å) [51] is a comparatively covalent compound; this reference exhibits the $K\beta_{1,3}$ peak shifted to the lowest energy (7058.97 eV). Compared to $FePO_4$, $FePO_4.2H_2O$ is slightly more ionic, with an average Fe-O bond distances of (~ 2.00 Å) [60]. This results in an intermediate position of $K\beta_{1,3}$ peak for $FePO_4.2H_2O$ (at 7059.20 eV).

In Fig. 4b all the spectra seem identical although the $K\beta_{1,3}$ peak in the Fe/H-ZSM-5 sample is slightly shifted to higher energies (i.e. $K\beta_{1,3}$ maxima at 7059.15 eV while for the rest of the references is at 7058.78 eV). This shift could indicate a different, more ionic, metal-ligand bond character with respect to the other samples. This could be a consequence of the fact that Fe is providing charge compensation of the

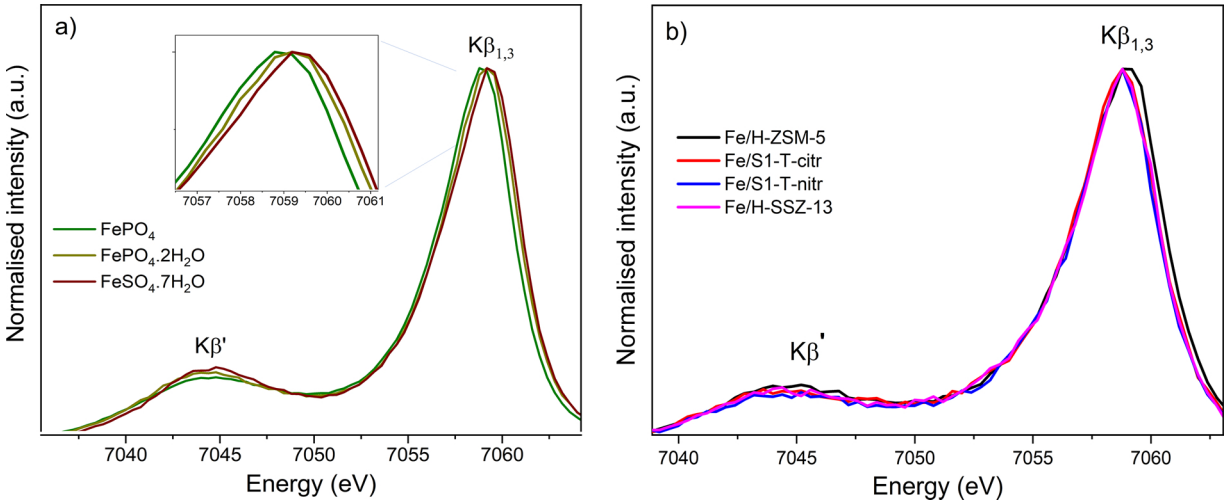

Fig. 4. Kβ XES mainlines for: a) Fe references at room temperature and b) Fe/zeolites acquired at room temperature after the activation (20% O_2/He flow, 2 h at 500 °C).

framework AlO_4^- charge. This is not the case of Fe/S1-T catalysts as these materials do not contain framework Al, while for Fe/H-SSZ-13 the majority of the species present are Fe_2O_3 particles.

3.2.2. HERFD-XANES and XES studies of Fe/zeolites under controlled gas atmosphere

In order to gain information on the Fe environment under different gas compositions, HERFD-XANES and XES spectra were collected for the catalysts exposed to: 1) 20% O_2 in He flow at 500 °C after activation, 2) 0.1% NO in He at 200 °C, 3) 1% NH_3 in He at 200 °C and 4) SCR conditions (5000 ppm NO, 5000 ppm NH_3 and 5% O_2 in He) at 300 °C.

Fig. 5a shows the HERFD-XANES spectra collected for Fe/H-ZSM-5 while Fig. 5b compares the pre-edge features with those for reference compounds. The scatter plots of pre-edge integrated areas vs. the area-based average centroid positions resulting from the pre-edge analysis is shown in Fig. 6; the corresponding deconvolution plots can be found in Fig. S5 while pre-edge feature values obtained from the analysis are presented in Table S2 in the ESI.

The HERFD-XANES data reveal a dynamic chemical state of Fe in Fe/H-ZSM-5 which changes with gas atmosphere. As discussed earlier, pre-edge peak features of the calcined catalyst suggest the presence of mainly isolated Fe^{3+} species with both Oh and Td species. No significant changes in the XANES spectrum can be observed when flowing NO (Fig. 5). While previous standard XANES studies show no reduction of Fe/zeolites under NO [28], Boubnov et al. [18] report very small shifts to lower energies (~ 0.05 eV) in the pre-edge peak centroid position using HERFD-XANES together with an increase in Fe co-ordination. They attribute these observations to NO adsorption onto Fe^{3+} centres, leading to Fe reduction (i.e. NO oxidative activation). Comparing the centroid positions for our calcined and NO exposed catalyst, no such shift is discernible. The slightly increased rising absorption edge energy and white line intensity in the NO exposed spectra (Fig. 5a) could be indicative of increased Fe coordination due to NO adsorption into Fe centres. This is not compelling evidence since the changes are within the error limits of the technique; nonetheless, this is consistent with those reported previously for Fe and Cu-based catalysts [18,61].

In contrast, the pre-edge peak is seen to shift to lower energies under NH_3 (centroid position goes from 7113.42 to 7112.95 eV), indicating reduction to Fe^{2+} - probably due to ammonia coordination to the metal and donation of the free electron pair of the nitrogen resulting in the formation of Fe^{2+}-NH_2 complexes. A similar shift is observed under NH_3-SCR conditions, pointing out that reoxidation of Fe^{2+} to Fe^{3+} during reaction is slow. In line with previous proposals [20,21]

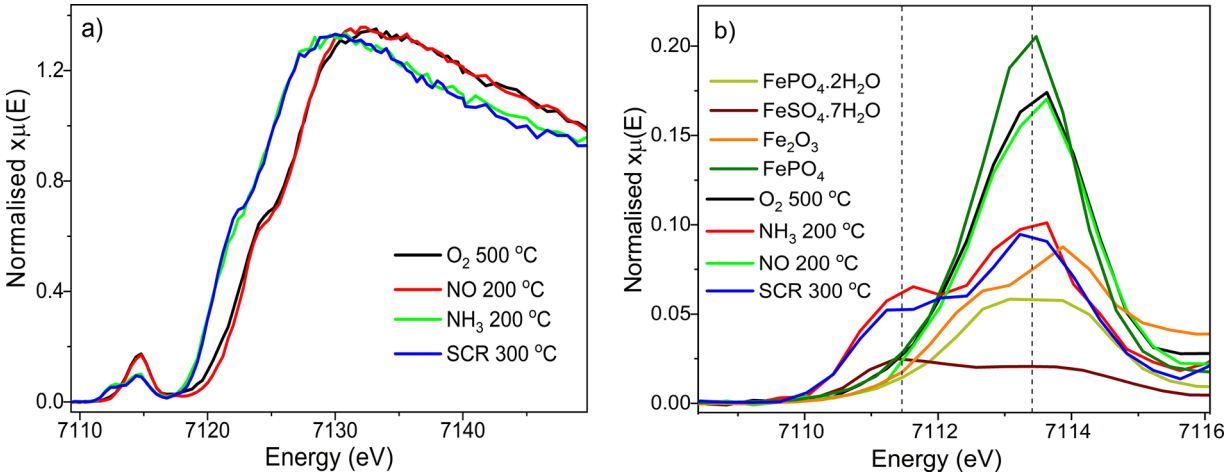

Fig. 5. a) Fe K-edge HERFD-XANES spectra collected for Fe/H-ZSM-5 after activation in 20% O_2/He (500 °C), under 0.1% NO/He and 1% NH_3/He (200 °C), and under SCR conditions (5% O_2, 5000 ppm NO, 5000 ppm NH_3 in He, 300 °C); a) General features for the catalyst spectra, and b) comparison of the pre-edge features for the Fe reference model compounds and the catalyst (dotted vertical line at 7111.4 and 7113.5 eV indicate the energy position of the two components in Fe^{2+} reference).

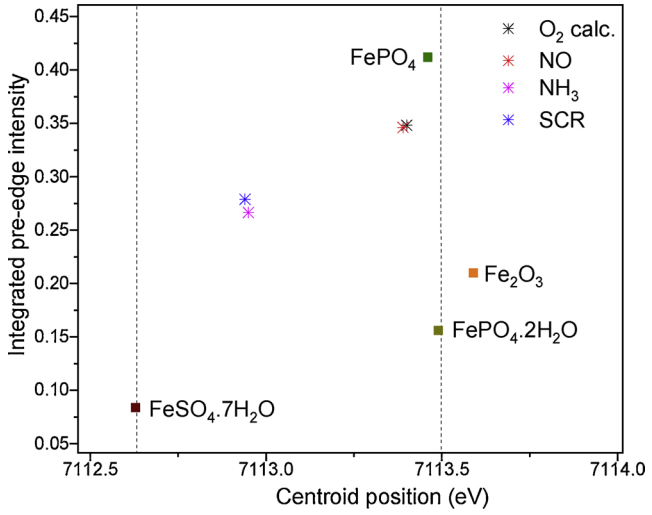

Fig. 6. Pre-edge integrated area vs the area-based average centroid for Fe in selected reference compounds and in Fe/H-ZSM-5 under in situ and operando conditions. Dotted vertical line at 7112.6 and 7113.5 eV indicate the average energy position of the centroid for Fe^{2+} and Fe^{3+} compounds respectively.

this might suggest that reoxidation of Fe sites is the rate-determining step for standard SCR. Note that MS spectrometry data collected during NH_3-SCR verified the correct operation of the catalysts with N_2 and H_2O product formation; this data can be found in Fig. S11 of the ESI.

Interestingly, the pre-edge features of Fe/H-ZSM-5 under NH_3 and SCR conditions indicate that only part of the Fe species are reduced to Fe^{2+}. As shown in Fig. 5a the relative intensities of the two pre-edge components (centred at 7111.6 and 7113.5 eV) in the reduced Fe/H-ZSM-5 and in $FeSO_4.7H_2O$ are inverted. The increased intensity of the high energy component in the spectra evidences the presence of Fe^{3+} species. In agreement, the centroid position for Fe/H-ZSM-5 under NH_3 and SCR appears located at higher energies than for the ferric reference compounds. Previous studies point to a linear response of the pre-edge centroid energy with the oxidation state [52]. Hence, using the same approach as in Equation S1 discussed earlier, a rough estimation of the reduction to Fe^{2+} can be performed using the centroid position of calcined Fe/H-ZSM-5 (7114.42 eV) and $FeSO_4.7H_2O$ reference (7112.64 eV) as the references for Fe^{3+} and Fe^{2+} species in the catalyst. The approximate estimation for Fe/H-ZSM-5 under SCR conditions (pre-edge centroid at 7112.95 eV) suggests that around 60% of species undergo reduction to Fe^{2+}.

From the data we cannot unequivocally discern and quantify the different possible geometries for Fe^{2+} and Fe^{3+} species in reduced Fe/H-ZSM-5. Recent in situ electron paramagnetic resonance (EPR) studies highlight that isolated octahedral Fe^{3+} sites in ion-exchanged Fe/zeolites are more reducible than tetrahedral sites [62]. In this regard, we can hypothesise that the Oh Fe^{3+} fraction of our samples is being reduced under reaction conditions used here while the Td Fe^{3+} remains oxidised.

Note the integrated pre-edge intensity of reduced Fe/H-ZSM-5 (around 0.27) is significantly higher than $FeSO_4.7H_2O$ (0.08). This is also the case when considering just the first pre-edge component around 7112.6 eV contributed only by the Fe^{2+} fraction of the Fe species. This intensity increase suggests a more distorted geometry of Fe^{2+} species in the catalyst. Alternatively, the state of the Fe^{2+} species can be regarded as a local geometry with coordination number of ca. 5 as proposed by Bouvnov et al. [18].

The Kβ main emission lines of Fe/H-ZSM-5 collected during the in situ and operando conditions (Fig. S6 in the ESI) exhibit no noticeable changes to account for variations in covalency under different gas compositions studied. Thus, at this stage we cannot readily correlate the XES lines with a Fe ionicity feature that could actively participate during SCR reaction.

Regarding the other three catalysts studied, Fe/S1-T-citr, Fe-S1-T-nitr and Fe/H-SSZ-13, the in situ and operando HERFD-XANES spectra presented only minor changes under the different gas environments studied (see Fig. 7a). The deconvolution results and pre-edge integrated area vs centroid plot for Fe/S1-T-citr, Fe/S1-T-nitr an Fe/H-SSZ-13 is shown in the ESI (Fig. S7 to S10 and Table S2); the plot presents only small shifts that are within the analysis error. No significant changes are seen either in the Kβ mainlines (Fig. 7b).

The fact that no reduction is observed in these three samples suggests a decreased redox activity of the Fe species. This is expected for Fe_xO_y clusters and large Fe_2O_3 particles (main species in Fe/S1-T-nitr and Fe/H-SSZ-13), which, by having a lower number of accessible sites for adsorption, should have a lower activity for SCR at low temperatures [11–13]. In case of the isolated Td Fe^{3+} species it needs to be considered that isomorphously substituted Td Fe^{3+} in Silicalite-1 would be less accessible to reactants than extraframework Fe species. This is due to the fact that substituted Fe sites are shielded and stabilised by the zeolite framework [49,63].

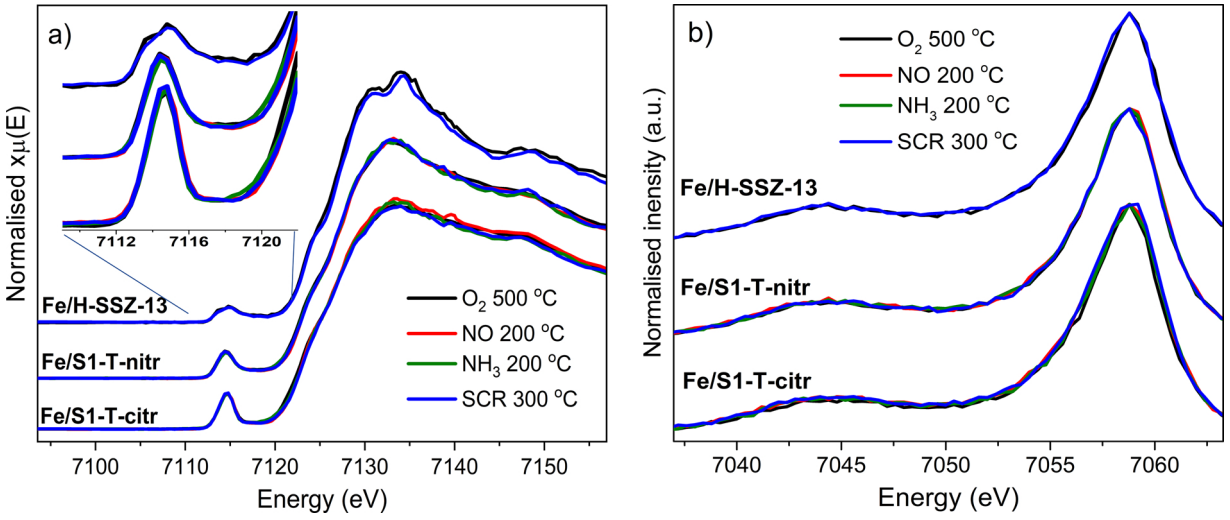

Fig. 7. Fe/S1-T-citr, Fe/S1-T-nitr and Fe/H-SSZ-13 spectra acquired after activation (20% O_2/He, 500 °C) under NO (0.1% NO/He, 200 °C), under NH_3 (1% NH_3/He, 200 °C) and under SCR conditions (5% O_2, 5000 pm NO, 5000 ppm NH_3 in He, 300 °C): a) Fe K-edge HERFD-XANES, and b) Fe Kβ emission mainlines.

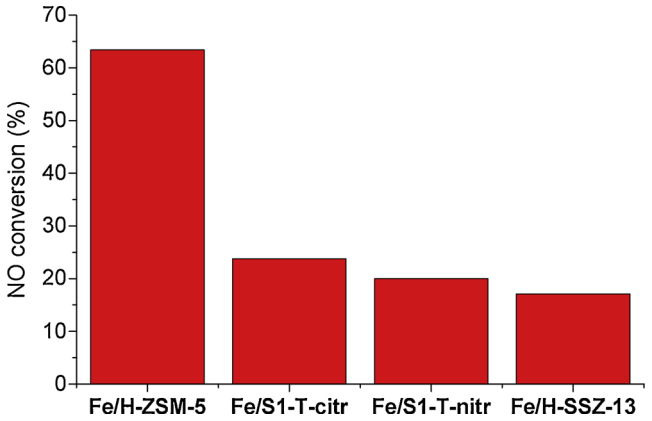

Fig. 8. NO conversion of Fe/zeolites after 1 h of NH_3-SCR under 5000 ppm NO, 5000 ppm NH_3 and 5% O_2 flow at 300 °C, GHSV = 35,000 h^{-1}.

3.3. Standard NH_3-SCR catalytic results for Fe/zeolites

To obtain quantitative catalytic data, the NH_3-SCR activity of Fe/zeolites at 300 °C was evaluated via lab-based measurements. The NO conversion values obtained for the Fe/zeolites after one hour of reaction (Fig. 8) result in the following trend: Fe/H-ZSM-5 (63.4%) > Fe/S1-T-citr (23.8%) > Fe/S1-T-nitr (20.0%) > Fe/H-SSZ-13 (17.1%). Note that the results show formation of N_2 and H_2O products while no N_2O side product is detected (mass spectrometry trends for the reaction products is given in Fig. S12 in ESI).

The conversion trends suggest that isolated Fe species are the most active centres for NH_3-SCR at 300 °C while clusters and large Fe_2O_3 particles show lower NH_3-SCR performance.

Interestingly, Fe/H-ZSM-5 presents significantly higher NO conversion than the other samples studied. In spite of the differences in Fe species distribution, activity for Fe/S1-T-citr, Fe/S1-T-nitr and Fe/H-SSZ-13 show moderate variations. Even Fe/S1-T-citr, dominated by isolated Td Fe^{3+} centres, gives nearly three times less NO conversion than Fe/H-ZSM-5. The lower activity in these samples can be related with the decreased Fe reducibility observed by HERFD-XANES. The results for Fe/S1-T-citr, showing a good Fe dispersion, can be rationalised if we consider that isolated Td Fe^{3+} are occupying framework positions, resulting in highly stable FeO_4 tetrahedra. Framework Fe is known to be more difficult to reduce as it is stabilised and shielded by the zeolite [49,63]. In agreement, extra framework isolated Fe sites have been reported to be more active for NH_3-SCR than isomorphously substituted Fe species [63,64]. It is very likely that small clusters are the responsible of the activity observed on Fe/S1-T-citr, Fe/S1-T-nitr and Fe/H-SSZ-13, with the differences in activity among them being probably due to a particle size effect.

Hence, our data indicates that optimal NH_3-SCR activity in Fe/H-ZSM-5 is given by highly reducible isolated Oh Fe^{3+} species. The presence of framework Al and the resulting ion exchange capacity of H-ZSM-5 is probably the driving force for the formation of these highly active Fe centres. Indeed, it has been suggested that partial compensation of the positive charge of ion exchanged Fe species by the local negative charge likely facilitates the Fe^{3+}/Fe^{2+} redox cycle resulting in high catalytic activity in NH_3-SCR [3]. Nonetheless, most of Fe in this catalyst is agglomerated as Fe_2O_3 particles in the zeolite outer surface which explains its low activity.

4. Conclusions

Fe/zeolites (c.a. 0.5 wt. %) have been synthesised by incipient wetness impregnation using H-ZSM-5, Silicalite-1 and H-SSZ-13 zeolites as supports. The samples have been characterised by UV–vis and HERFD-XANES and XES. Changes in Fe chemical state under O_2, NO and NH_3 atmosphere as well as under SCR conditions have been studied by in situ and operando HERFD-XANES and XES. The main results of these studies can be summarised as follows:

- The preparation methods used led to catalysts with varied Fe species. Fe/H-ZSM-5 comprises isolated Fe^{3+} species with both Oh and Td geometries. Fe/Silicalite-1 prepared with ferric citrate contains highly dispersed Fe species, mainly in tetrahedral coordination, while Fe/Silicalite-1 prepared with ferric nitrate presents increased amounts of Fe_xO_y clusters and Fe_2O_3 particles. Fe/H-SSZ-13 catalyst comprises mainly large Fe_2O_3 particles. Unlike the other catalysts studied, Fe/H-ZSM-5 presents a slight shift of the $K\beta_{1,3}$ X-ray emission peak to lower energies suggesting a more ionic metal-ligand (Fe-O) bond character. While this could be induced by a charge compensating effect between Fe^{3+} and framework AlO_4^-, the absence of detectable changes in $K\beta_{1,3}$ under reaction condition does not allow to see a correlation between the increased ionicity and SCR mechanism.
- Changes in the spectra during in situ HERFD-XANES measurements were only observed for Fe/H-ZSM-5. The increase in white line intensity upon NO exposure could suggests an increase in Fe coordination due to NO adsorption on Fe centres. Exposing the catalyst to NH_3 flow or SCR conditions results in partial reduction to Fe^{2+}. It is hypothesised that isolated Oh Fe species undergo reduction while Td species remain oxidised.
- Fe/H-ZSM-5 gives higher NH_3-SCR activity, this can be attributed to the isolated Oh Fe^{+3} species with enhanced redox behaviour. The presence of framework Al appears to promote the formation of such species in ion exchange sites probably providing charge compensation facilitating Fe redox activity. The absence of spectral changes in Fe/S1-T catalysts points that Td Fe^{3+} species barely interact with the reactants, showing no reduction. The activity in these samples is attributed to the presence of Fe clusters/particles.

These observations suggest that the reducibility of Fe and its capacity to coordinate with reactant gases is important for realising low-temperature activity which is essential during cold-start/idling of vehicles. Cu-based catalysts are usually the choice for low temperature SCR; they show appreciable activity (100% NO conversion) already at 200 °C while Fe-based catalysts require at least 300 °C [2]. Nonetheless, for its industrial use, Fe is cheaper than Cu and there are no reported issues with its use in such technology on a global scale. Perhaps then, understanding how the reducibility of Fe can be further affected is key to realising low temperature activity of these catalysts for the standard SCR reaction.

Acknowledgments

This study received financial support from EPSRC (EPK, a UCL Impact PhD award, Diamond Light Source and Johnson Matthey). This research used resources from RCaH and Johnson Matthey Technology Centre. EPSRC is also acknowledged for sponsoring the UK Catalysis Hub which provided resources and support via grants EP/K014706/1, EP/K014668/1, EP/K014854/1, EP/K014714/1 and EP/I019693/1 and for an Early Career Fellowship for AMB (EP/K007467/1). Diamond Light Source is thanked for the awarded beamtime (SP9925-2).

Appendix A. Supplementary data

Supplementary material related to this article can be found, in the online version, at doi:https://doi.org/10.1016/j.apcata.2018.11.026.

References

[1] S. Brandenberger, A. Tissler, R. Althoff, O. Kröcher, Catal. Rev. 50 (2008) 492–531.
[2] A.M. Beale, F. Gao, I. Lezcano-Gonzalez, C.H.F. Peden, J. Szanyi, Chem. Soc. Rev.

44 (2015) 7371–7405.
[3] P. Sazama, B. Wichterlová, E. Tábor, P. Šťastný, N.K. Sathu, Z. Sobalík, J. Dědeček, Š. Sklenák, P. Klein, A. Vondrová, J. Catal. 312 (2014) 123–138.
[4] M. Iwasaki, K. Yamazaki, K. Banno, H. Shinjoh, J. Catal. 260 (2008) 205–216.
[5] S. Brandenberger, O. Kröcher, A. Tissler, R. Althoff, Ind. Eng. Chem. Res. 50 (2011) 4308–4319.
[6] M. Santhosh Kumar, M. Schwidder, W. Grünert, A. Brückner, J. Catal. 227 (2004) 384–397.
[7] R.Q. Long, R.T. Yang, J. Catal. 188 (1999) 332–339.
[8] R.Q. Long, R.T. Yang, Catal. Lett. 74 (2001) 201–205.
[9] F. Liu, W. Shan, Z. Lian, J. Liu, H. He, Appl. Catal. B Environ. 230 (2018) 165–176.
[10] E. Yuan, G. Wu, W. Dai, N. Guan ab, L. Li, Catal. Sci. Technol. 7 (2017) 3036.
[11] H. Liu, J. Wang, T. Yu, S. Fan, M. Shen, Catal. Sci. Technol. 4 (2014) 1350–1356.
[12] M. Schwidder, M. Santhosh Kumar, A. Brückner, W. Grünert, Chem. Commun. (2005) 805–807.
[13] S. Brandenberger, O. Kröcher, A. Tissler, R. Althoff, Appl. Catal. B, Environ. 95 (2010) 348–357.
[14] M. Schwidder, M.S. Kumar, K. Klementiev, M.M. Pohl, A. Brückner, W. Grünert, J. Catal. 231 (2005) 314–330.
[15] Q. Sun, Z.-X. Gao, H.-Y. Chen, W.M. Sachtler, J. Catal. 201 (2001) 89–99.
[16] H.-Y. Chen, E.-M. El-Malki, X. Wang, R.A. Van Santen, W.M.H. Sachtler, J. Mol. Catal. A Chem. 162 (2000) 159–174.
[17] M. Høj, M.J. Beier, J.-D. Grunwaldt, S. Dahl, Appl. Catal. B Environ. 93 (2009) 166–176.
[18] A. Boubnov, H.W.P. Carvalho, D.E. Doronkin, T. Gunter, E. Gallo, A.J. Atkins, C.R. Jacob, J.D. Grunwaldt, J. Am. Chem. Soc. 136 (2014) 13006–13015.
[19] P.S. Metkar, N. Salazar, R. Muncrief, V. Balakotaiah, M.P. Harold, Appl. Catal. B Environ. 104 (2011) 110–126.
[20] M.P. Ruggeri, A. Grossale, I. Nova, E. Tronconi, H. Jirglova, Z. Sobalik, Catal. Today 184 (2012) 107–114.
[21] T.C. Bruggemann, F.J. Keil, J. Phys. Chem. C 115 (2011) 23854–23870.
[22] M. Devadas, O. Kröcher, M. Elsener, A. Wokaun, N. Söger, M. Pfeifer, Y. Demel, L. Mussmann, Appl. Catal. B Environ. 67 (2006) 187–196.
[23] K. Rahkamaa-Tolonen, T. Maunula, M. Lomma, M. Huuhtanen, R.L. Keiski, Catal. Today 100 (2005) 217–222.
[24] R.Q. Long, R.T. Yang, J. Catal. 207 (2002) 224–231.
[25] H.Y. Huang, R.Q. Long, R.T. Yang, Appl. Catal. A Gen. 235 (2002) 241–251.
[26] I. Ellmers, R.P. Vélez, U. Bentrup, A. Brückner, W. Grünert, J. Catal. 311 (2014) 199–211.
[27] M. Schwidder, M. Santhosh Kumar, U. Bentrup, J. Pérez-Ramírez, A. Brückner, W. Grünert, Microporous Mesoporous Mater. 111 (2008) 124–133.
[28] D. Klukowski, P. Balle, B. Geiger, S. Wagloehner, S. Kureti, B. Kimmerle, A. Baiker, J.-D. Grunwaldt, Appl. Catal. B Environ. 93 (2009) 185–193.
[29] M. Li, Y. Yeom, E. Weitz, W.M.H. Sachtler, Catal. Lett. 112 (2006) 129–132.
[30] S. Brandenberger, O. Kröcher, A. Wokaun, A. Tissler, R. Althoff, J. Catal. 268 (2009) 297–306.
[31] N.A. Grosso-Giordano, A.J. Yeh, A. Okrut, D.J. Xiao, F. Grandjean, G.J. Long, S.I. Zones, A. Katz, Chem. Mater. 29 (2017) 6480–6492.
[32] M. Wilke, F. Farges, P.-M. Petit, G.E. Brown JR, F. Martin, Am. Miner. 86 (2001) 714–730.
[33] T.E. Westre, P. Kennepohl, J.G. Dewitt, B. Hedman, K.O. Hodgson, E.I. Solomon, J. Am. Chem. Soc. 119 (1977) 6297–6314.
[34] A. Boubnov, H. Lichtenberg, S. Mangold, J.D. Grunwaldt, J. Synchrotron Radiat. 22 (2015) 410–426.
[35] W.M. Heijboer, P. Glatzel, K.R. Sawant, R.F. Lobo, U. Bergmann, R. a Barrea, D.C. Koningsberger, B.M. Weckhuysen, F.M.F. de Groot, J. Phys. Chem. B 108 (2004) 10002–10011.
[36] M. Bauer, Phys. Chem. Chem. Phys. 16 (2014) 13827–13837.
[37] K. Hamalainen, D.P. Siddons, J.B. Hastings, L.E. Berman, Phys. Rev. Lett. 67 (1991) 2850–2853.
[38] C.J. Pollock, M.U. Delgado-Jaime, M. Atanasov, F. Neese, S. DeBeer, J. Am. Chem. Soc. 136 (2014) 9453–9463.
[39] D.D. Kragten, J.M. Fedeyko, K.R. Sawant, J.D. Rimer, D.G. Vlachos, R.F. Lobo, M. Tsapatsis, J. Phys. Chem. B 107 (2003) 10006–10016.
[40] Y. Bu, Y. Wang, Y. Zhang, L. Wanga, Z. Mi, W. Wub, E. Min, S. Fu, Catal. Commun. 8 (2007) 16–20.
[41] A.M. Beale, I. Lezcano-Gonzalez, W.A. Slawinksi, D.S. Wragg, Chem. Commun. 52 (2016) 6170–6173.
[42] M. Moliner, C. Franch, E. Palomares, M. Grill, A. Corma, Chem. Commun. 48 (2012) 8264–8266.
[43] M.J. Díaz-Cabañas, P.A. Barrett, M.A. Camblor, Chem. Commun. (1998) 1881–1882.
[44] S. Diaz-Moreno, M. Amboage, M. Basham, R. Boada, N.E. Bricknell, G. Cibin, T.M. Cobb, J. Filik, A. Freeman, K. Geraki, D. Gianolio, S. Hayama, K. Ignatyev, L. Keenan, I. Mikulska, J.F.W. Mosselmans, J.J. Mudd, S.A. Parry, J. Synchrotron Radiat. 25 (2018) 998–1009.
[45] S. Diaz-Moreno, S. Hayama, M. Amboage, A. Freeman, J. Sutter, G. Duller, J. Phys. Conf. Ser. 190 (2009) 12038.
[46] S. Hayama, G. Duller, J.P. Sutter, M. Amboage, R. Boada, A. Freeman, L. Keenan, B. Nutter, L. Cahill, P. Leicester, B. Kemp, N. Rubies, S. Diaz-Moreno, J. Synchrotron Radiat. 25 (2018) 1556–1564.
[47] H.H. Johann, L. Bonn, Physik 69 (1931) 185–206.
[48] B. Ravel, M. Newville, J. Synchrotron Radiat. 12 (2005) 537–541.
[49] S. Bordiga, R. Buzzoni, F. Geobaldo, C. Lamberti, E. Giamello, A. Zecchina, G. Leofanti, G. Petrini, G. Tozzola, G. Vlaic, J. Catal. 158 (1996) 486–501.
[50] M. Matzapetakis, C.P. Raptopoulou, A. Tsohos, V. Papaefthymiou, N. Moon, A. Salifoglou, J. Am. Chem. Soc. 120 (1998) 13266–13267.
[51] A. Sanson, O. Mathon, S. Pascarelli, J. Chem. Phys. 140 (2014) 224504–144305.
[52] A. Ceglia, G. Nuyts, S. Cagno, W. Meulebroeck, K. Baert, P. Cosyns, K. Nys, H. Thienpont, K. Janssens, H. Terryn, Anal. Methods 6 (2014) 2662–2671.
[53] K. Taxer, H. Bartl, Cryst. Res. Technol. 39 (2004) 1080–1088.
[54] L.J. Lobree, I. Hwang, J.A. Reimer, A.T. Bell, J. Catal. 186 (1999) 242–253.
[55] S.H. Choi, B.R. Wood, J.A. Ryder, A.T. Bell, J. Phys. Chem. 107 (2003) 11843–11851.
[56] E.A. Pidko, E.J.M. Hensen, R.A. Van Santen, Proc. R. Soc. A 468 (2012) 2070–2086.
[57] Y.I. Joe, G.C.O. 'neil, L. Miaja-Avila, J.W. Fowler, R. Jimenez, K.L. Silverman, D.S. Swetz, J.N. Ullom, J. Phys. B At. Mol. Opt. Phys. 49 (2015) 024003.
[58] A.P. Grosvenor, B.A. Kobe, M.C. Biesinger, N.S. Mcintyre, Surf. Interface Anal. 36 (2004) 1564–1574.
[59] W.H. Baur, Acta Crystallogr. 17 (1964) 1167–1174.
[60] G. Sankar, J.M. Thomas, C.R.A. Catlow, Top. Catal. 10 (2000) 255–264.
[61] I. Lezcano-Gonzalez, D.S. Wragg, W.A. Slawinski, K. Hemelsoet, A. Van Yperen-De Deyne, M. Waroquier, V. Van Speybroeck, A.M. Beale, J. Phys. Chem. C 119 (2015) 24393–24403.
[62] H. Liu, J. Wang, T. Yu, S. Fan, M. Shen, Catal. Sci. Technol. 4 (2014) 1350–1356.
[63] J. Perez-Ramırez, G. Mul, F. Kapteijn, J.A. Moulijn, A.R. Overweg, A. Domenech, A. Ribera, I.W.C.E. Arends, J. Catal. 207 (2002) 113–126.
[64] A. Mette, F. Ae, S. Mert, A.E. Johannes, D.-H. Ae, R. Fehrmann, A.E. Claus, H. Christensen, Catal. Lett. 130 (2009) 1–8.